Title: Cutaneous jet-injection of naked mRNA vaccine induces robust immune responses without systemic vaccine spillage

Saed Abbasi[1#], Miki Matsui-Masai[2#], Akimasa Hayashi[3], Theofilus A. Tockary[1], Shiro Akinaga[2], Kazunori Kataoka*[1] and Satoshi Uchida*[1,4]

#: Equal contribution

[1] Innovation Center of NanoMedicine (iCONM), Kawasaki Institute of Industrial Promotion, 3-25-14 Tonomachi, Kawasaki-ku, Kawasaki, 210-0821, Japan

[2] Department of Research, NanoCarrier Co., Ltd., 3-25-14 Tonomachi, Kawasaki-ku, Kawasaki, 210-0821, Japan

[3] Department of Pathology, Kyorin University School of Medicine, 6-20-2 Shinkawa, Mitaka-shi, Tokyo, 181-8611, Japan

[4] Department of Advanced Nanomedical Engineering, Medical Research Institute, Tokyo Medical and Dental University (TMDU), 1-5-45 Yushima Bunkyo-ku Tokyo 113-8510 Japan

* Correspondence to Kazunori Kataoka, Satoshi Uchida
Email: kkataoka@g.ecc.u-tokyo.ac.jp (K.K.), uchida.anme@tmd.ac.jp (S.U.)

Abstract

Locally injected lipid nanoparticle (LNP)-based mRNA vaccines migrate systemically, which could raise safety concerns. From a mechanistic viewpoint, whether local or systemic antigen expression contributes to the vaccine effects remains unclear. Herein, we localized the antigen protein expression using naked mRNA and drastically improved the delivery efficiency in the skin by jet injection. Consequently, jet-injected naked mRNA outperformed a widely-used LNP in humoral immunity induction at the highest tolerable mRNA doses of each formulation in mice. A mechanistic investigation suggests that antigen-presenting cells taking up antigens at the jet-injection site of naked mRNA migrate to draining lymph nodes, enabling robust immunization without systemic mRNA distribution. Ultimately, jet injection of SARS-CoV-2 spike mRNA provided efficient antibody responses, neutralizing potential and cellular immunity in rodents and non-human primates with no reactogenicity. Conclusively, naked mRNA jet injection is a robust, tolerable, and simple vaccine candidate.

Introduction

The use of antigen-encoding messenger RNA (mRNA) has instigated a paradigm shift in vaccine development because of the high efficacy of mRNA vaccine and the ease of mRNA sequence designing and production (*1, 2*). In 2020, two novel mRNA vaccines, BNT162b2 and mRNA-1273, gained emergency approval for use against the coronavirus disease 2019 (COVID-19), showing >90% effectiveness in preventing the symptomatic disease (*3-6*). Both vaccines employ lipid nanoparticles (LNPs) to protect mRNA against enzymatic degradation and enhance its intracellular delivery following intramuscular (i.m.) injection. Notably, locally injected mRNA LNP migrates beyond the injection site to produce considerable levels of the encoded antigen in other tissues, including the draining lymph nodes (dLNs), spleens, and livers, because of LNP tropism to these tissues and mRNA protection from nuclease attack (*7-10*). Previous research suggests that mRNA-LNP migration to dLN is critical for inducing a persistent antibody response against COVID-19 (*11, 12*). However, the systemic distribution of LNPs has potential safety concerns, which are under extensive investigation (*13, 14*). Further, the multifaceted nature of mRNA-LNPs in orchestrating the immune response at both the injection site and lymphoid organs complicates our understanding of mRNA vaccine mechanisms. Therefore, separating the local and systemic effects would be beneficial from both safety and mechanistic understanding viewpoints.

Injecting naked mRNA without any delivery carrier could localize mRNA distribution to the injection site because rapid enzymatic degradation would prevent mRNA from migrating to other tissues in an intact form (*15*). However, the efficient introduction of naked mRNA into immune cells, especially antigen-presenting cells (APCs), is a prerequisite. The skin is a favorable vaccination site because the epidermis and dermis are rich in APCs, which reside at a density higher than the muscle tissue (*16, 17*). Previous studies of infectious disease mRNA vaccines demonstrated the utility of the i.d. route in non-human primates (NHPs) and humans using protamine- or LNP-based mRNA formulations (*18-20*). In recent clinical trials of BNT162b2 and mRNA-1273, the i.d. route required only 1/10 - 1/5 of mRNA dose compared to the i.m. route to produce a comparable humoral and cellular immunity, with a trend of alleviated adverse effects (*21-23*). Despite the potential of i.d. route in mRNA vaccines, i.d. delivery of naked mRNA induced low antibody responses and moderate CD8+ responses (*24-26*), limiting its application to cancer vaccination.

Plausible mechanisms of the poor vaccination outcomes after i.d. injection of naked mRNA include the rapid mRNA degradation in the dermal tissue (*27*) and the large size and highly negative charge of mRNA limiting its cell entry. Herein, we used a novel needle-free, pyro-drive liquid jet injector (PYRO) (*28*) to deliver naked mRNA instantaneously and efficiently in the skin before considerable mRNA degradation. According to previous research, PYRO enhanced plasmid DNA (pDNA) delivery to rodent skin, providing efficient vaccination effects (*29-31*). Interestingly, in the present study, PYRO effectively

delivered naked mRNA in the skin of rodents and NHPs, despite a 100-fold faster mRNA degradation rate by nucleases in extracellular fluids than pDNA (*32*). More importantly, PYRO injection of naked mRNA provided strictly localized protein expression at the injection site, reducing systemic toxicity compared to mRNA-LNPs. This distribution profile allowed us to study the contribution of local antigen expression on vaccination effects, independently from that at dLN, spleens, or livers. Consequently, we show for the first time that the localized antigen expression at the injection site is sufficient to induce humoral and cellular immunity at an intensity close to that obtained by LNP-mRNA vaccines. Furthermore, our approach demonstrated its utility in vaccination against SARS-CoV-2 spike protein in mice and NHPs. Thus, naked mRNA jet injection provides a simple and safe option for mRNA vaccine clinical development by avoiding systemic vaccine spillage.

Results

1. PYRO boosts naked mRNA delivery efficiency in the skin.

The protein expression level in the skin following i.d. injection of *firefly luciferase* (*fLuc*)-encoding mRNA was evaluated in two mice strains: Balb/C (**Figure 1a**) and C57BL/6J (**Figure 1b**). In both mice strains, PYRO injection gave approximately 10 – 100-fold more efficient fLuc expression at the injection site than a manual injection with a needle and a syringe (N&S). Interestingly, PYRO injection provided a smaller distribution area of mRNA solution than N&S injection (**Figures 1c, d)**, despite its much higher capability for mRNA introduction. This observation suggests that high pressure produced by the jet injector may facilitate mRNA internalization to the cells in a confined space. At microscopic levels, N&S damaged the tissue on a broader area than PYRO injection in the H&E-stained histological sections, causing dermal necrosis and subcutaneous inflammation (**Figures 1e, f)**. Needle insertion may explain the damage in N&S. Then, we observed tissue distribution of protein expression after PYRO injection of *GFP*-encoding mRNA. The cells in the approximately 1-mm-wide area at the injection site showed GFP expression (**Figure 1g**, solid rectangle). GFP-positive cells included CD11c-positive dendritic cells stained in yellow in **Figure 1h**, demonstrating successful mRNA delivery to APCs by PYRO injection.

2. PYRO provides localized protein expression in the skin.

We next compared the systemic distribution of protein expression and mRNA between naked mRNA PYRO injection and LNP N&S injection into mouse skin. Throughout this study, we used the MC3 ionizable lipid LNP as a representative mRNA-LNP since it is widely used in vaccination studies (*8*). In whole-body IVIS imaging, LNP showed local fLuc expression in the skin and systemic expression in the other organs, while the expression was localized to the injection site after naked mRNA PYRO injection

(**Figure 2a**). The local fLuc expression levels on the skin were comparable between PYRO-injected naked mRNA and N&S injection of LNP (**Figure 2b**). For detailed analysis of biodistribution, fLuc expression levels were quantified in extracted tissues 24 h post-injection of *fLuc* mRNA. PYRO injection of naked mRNA exhibited undetectable fLuc signals in either the inguinal or axillary lymph nodes (LNs) on the same side (ipsilateral side) and the other side (contralateral side) of the injection (**Figure 2c**), the liver (**Figure 2d**), or the spleen (**Figure 2e**). On the contrary, i.d. N&S injection of *fLuc* mRNA formulated in LNP showed considerable protein expression in the ipsilateral inguinal and axillary LNs (**Figure 2c**) and the liver, and the spleen (**Figure 2d**) but not in the contralateral LNs.

Further, mRNA tissue distribution was directly observed independently from the intracellular translation by quantitative PCR (qPCR) of delivered mRNA 30 min and 4 h post-injection. We observed mRNA levels at time points earlier than 24 h to minimize the influence of mRNA degradation after tissue distribution (*33*). mRNA was undetectable in the ipsilateral inguinal and axillary LNs, spleen, and liver upon PYRO injection of 2 and 9 μg naked mRNA, while LNP showed widespread systemic distribution to these organs (**Figures 2f-i, Supplementary Figure S1**).

LNP may migrate to the lymph node via lymphatic vessels (*34*). Particles with the size of 10 – 200 nm are transported preferentially through lymphatic vessels (*35*) before they finally drain into blood vessels and systemic circulation. The mRNA-LNP particle had a size below 70 nm and a neutral surface charge (**Supplementary Table 1**), making their lymphatic transport expected. Once pooled in the bloodstream, the LNPs accumulated in other organs, such as the liver and spleen, as shown in **Figure 2d, e.** In contrast, naked mRNA, susceptible to rapid enzymatic degradation, failed to migrate beyond the injection site (**Figure 2a, c-i)**.

3. Naked mRNA does not induce systemic inflammatory responses.

The difference in distribution profiles between naked mRNA and LNP may influence systemic inflammatory responses after vaccination. We checked proinflammatory transcripts in systemic organs and LNs by qPCR. After PYRO injection of naked mRNA, transcript levels of IFN-β and IL-6 were comparable with those of untreated control in inguinal and axillary LNs, liver, or spleen, irrespective of the dose (**Figure 3**). This result is consistent with the lack of any measurable protein expression or mRNA distribution in these organs following naked mRNA PYRO injection (**Figure 2**). On the contrary, mRNA-LNP increased the expression of proinflammatory transcripts, especially at a high mRNA dose (9 μg). The inguinal LN on the ipsilateral side of injection, but not on the contralateral side, exhibited high inflammatory transcript expression after injection of 2 and 9 μg mRNA-LNPs **(Figure 3a, e)**. Furthermore, 9 μg mRNA-LNP induced inflammatory responses in the liver and spleen (**Figure 3c, d, g, h**), presumably because of LNP systemic distribution. Since the m1Ψ-modifed mRNA used in this experiment may be low immunogenic,

the observed inflammatory cytokine upregulation may be attributed to the immunogenic nature of lipids in the LNP (*36*). Nonetheless, a low-dose LNP (2 μg mRNA) was highly tolerable, inducing minimal proinflammatory transcripts in the liver and spleen (**Figure 3c, d, g, h**).

4. PYRO-injected naked mRNA induces robust humoral immunity against a model antigen.

We used OVA as a model antigen to evaluate antibody production in the first step. The mRNA dose was divided into two equal volumes (20 μL each) and injected in both sides of C57BL/6J mouse flanks each time. 9 μg naked *OVA* mRNA injected using PYRO in a prime-boost regimen produced OVA-specific IgG efficiently. In contrast, OVA-specific IgG was mostly undetectable after N&S injection of naked mRNA (**Figure 4a**). PYRO injection of naked *OVA* mRNA was also compared to i.d. N&S injection of *OVA* mRNA-LNP. The dose of mRNA-LNP was fixed at 2 μg mRNA because higher doses induced off-target systemic inflammatory responses in the liver and spleen (**Figure 3**). This result is consistent with a previous study, wherein mRNA-LNP was tolerable at doses 1 – 3 μg mRNA per dose but became toxic at doses 10 μg or higher, inducing significant weight loss in mice (*37*). Notably, the PYRO injection of 9 μg naked *OVA* mRNA induced a significantly higher anti-OVA IgG amount than the 2 μg mRNA-LNP (**Figure 4a**). Bearing in mind that only the LNP group, but not the PYRO injected naked mRNA, delivered a considerable amount of mRNA into dLNs (**Figure 2**), the results in **Figure 4a** highlight the capability of mRNA vaccines to induce robust humoral immunity even without mRNA migration to dLNs. Still, mRNA-LNP produced higher antibody production than PYRO-injected naked mRNA when injected at the same dose of 2 μg.

PYRO injection of 18 μg naked *OVA* mRNA as a single shot (prime only) failed to induce anti-OVA IgG as efficiently as observed in a prime and boost injection of 9 μg each time (**Figure 4a**). This result is consistent with previous findings, showing the benefit of a prime-boost protocol in vaccines (*38*). Besides C57BL6J mice, Balb/C mice exhibited efficient anti-OVA IgG production after PYRO injection of naked *OVA* mRNA (**Figure 4b**). In the evaluation of IgG isotypes, PYRO injection of naked *OVA* mRNA produced considerable amounts of IgG1 and IgG2a isotypes in C57BL6J and Balb/C mice (**Figure 4c, d, respectively**).

Next, we studied the injection position effects on prime and boost vaccinations, specifically clarifying whether the injection site should be the same for each prime and boost. Prime and boost PYRO injections were performed either ipsilaterally on one flank or contralaterally on both flanks. Mice receiving the boost dose at the ipsilateral side of the prime injection exhibited a slightly higher IgG amount than those receiving the two doses contralaterally (**Figure 4b**). This result could be explained by the immune stimulation of local dLNs by repeated injections in the same location (*39*). Note that the role of local dLNs after the PYRO injection is addressed below (see **Figure 4f, g**). Nonetheless, contralateral boosting still

produced considerable amounts of IgG (**Figure 4b**), indicating the robust systemic immunization induced by PYRO-injected naked mRNA. Despite the lack of specific recommendations on the side of injection for the prime and boost administration of COVID-19 mRNA-LNP vaccines in clinical settings, preliminary studies were carried out by injecting the animals on the same side for both prime and boost (*4, 40*).

Remarkably, jet-injected 9 μg naked mRNA induced higher levels of anti-OVA IgG than LNP loading 2 μg mRNA (**Figure 4a**), while only LNP, not naked mRNA, migrated to dLN (**Figures 3a,c**). These observations motivated us to investigate the mechanisms underlying PYRO-injected mRNA mounting an adaptive immune response even without mRNA migration to dLNs. APCs in the dermis and epidermis, including Langerhans cells, dermal DC, and macrophages, can take up and traffic the antigen to the dLN, presenting it to B and T cells for induction of immunity (*34, 41*). Although no luciferase signal was observed in dLNs 24 h post-injection (**Figure 2a**), bioluminescence imaging is not a sensitive method to track the migration of DCs *in vivo* if not combined with other imaging modalities (*42*). Hence, we observed the inguinal dLN 24 h post-jet-injection of naked *GFP* mRNA in the skin using microscopy. GFP-positive cells were observed in the dLN (**Figure 4f**), with many cells co-expressing CD11c, a DC activation marker (**Figure 4g**). This observation suggests that DCs taking up mRNA in the skin migrate from the skin to the dLN, wherein DCs may present antigens to T cells and B cells to induce robust humoral immune responses (**Figure 4a-c)**.

5. PYRO-injected naked mRNA induces robust cellular immunity against a model antigen.

PYRO injection also induced more efficient cellular immune responses against OVA than N&S injection in enzyme-linked immunospot (ELISpot) assay. Indeed, PYRO injection of 9 μg naked mRNA provided an approximately 5-fold higher number of OVA-specific IFN-γ-producing T cells in the spleens of vaccinated mice than N&S injection of the same dose mRNA (**Figure 5a**). Despite the efficient production of IFN-γ, a T-helper-1 (Th1)-related molecule, splenocytes of mice PYRO-injected with 9 μg naked mRNA produced a minimal amount of IL-4, a T-helper-2 (Th2)-related cytokine, after antigen stimulation (**Figure 5b**). This cytokine activation profile may benefit in reducing the risk of vaccine-associated enhanced diseases (*43*). Additionally, a single dose of 18 μg naked mRNA produced less efficient OVA-specific cellular immunity than a prime-boost series of 9 μg naked mRNA. This result further indicates the need for prime-boost dosing of sufficient mRNA doses. The 2 μg of mRNA injected in the LNP form provided an approximately 3-fold higher number of spots than PYRO-injected 9 μg naked mRNA although the latter outperformed the former in inducing humoral immunity (**Figure 4a**). Explaining the difference in magnitude between the cellular and humoral immunity induced by LNP and PYRO requires further investigation. Regarding the injection position effect of the prime and boost doses,

contralateral and ipsilateral boosting exhibited comparable induction of OVA-specific IFN-γ-producing T cells (**Figure 5c**).

6. PYRO-injected naked mRNA produces robust humoral and cellular immunity against Spike protein in rodents and NHPs.

Finally, we evaluated the feasibility of naked mRNA PYRO injection as a potential vaccine for COVID-19 in mice and NHPs. PYRO injection of naked *spike* mRNA at doses between 5 – 30 μg induced a strong total IgG production in Balb/C, with the highest level obtained at 30 μg (**Figures 6a**). Consistent with the *OVA* mRNA results, PYRO injection of 30 μg naked *spike* mRNA induced both IgG1 and IgG2a antibody isotypes (**Figure 6b**). The neutralization potential of mouse plasma was then tested by a surrogate virus neutralization test (sVNT), which evaluates the plasma capability to inhibit the interaction between the receptor-binding domain (RBD) of the SARS-CoV-2 spike protein and angiotensin-converting enzyme 2 (ACE2). Generally, data obtained from sVNT showed a positive correlation at high R^2 values with virus neutralization tests using SARS-CoV2 or pseudovirus coated with spike proteins (*44*). As shown in **Figure 6c**, PYRO-injected naked *spike* mRNA successfully inhibited the binding between RBD and ACE2 in all tested doses, indicating the strong potential of this method to induce viral neutralization. The blocking levels in **Figure 6c** remained approximately 50% at 100× plasma dilution, similar to the values obtained from the natural immunity in patients with prior COVID-19 (*44*). Finally, cellular immunity responses were evaluated by ELISpot assay of spleen samples (**Figure 6D**), showing a dose-dependent increase in spike protein-specific IFN-γ-producing T cells. Besides Balb/C mice, C57BL/6 mice also successfully produced IgG antibody against spike protein and spike-protein-reactive splenocytes (**Supplementary Figure S2**). These results demonstrate the advantage of jet injection to internalize a wide range of mRNA with different sizes and produce effective vaccination (4,247 nt for *spike* mRNA vs. 1,437 nt for *OVA* mRNA).

Further, the utility of naked mRNA PYRO injection was tested in NHPs. Cynomolgus monkeys received PYRO injection of naked mRNA solution three times every three weeks (**Figure 6e**). The injection volume was 50 μL per injection in monkeys and 20 μL in mice. Intriguingly, PYRO injected mRNA solution diffused horizontally in monkeys, with approximately 1 cm in diameter (**Figure 6f**). In contrast, the injection in mice provided only a 2 mm-sized area of diffusion (**Figure 6g**). The wide horizontal distribution of the mRNA solution in the dermal layer in monkeys is expected provide more efficient contact with APCs. Indeed, NHPs receiving 3 doses of 100 μg naked *spike* mRNA efficiently produced IgG antibodies against spike proteins **(Figure 6h**). The antibody titer peaked a week after the second dose and persisted at the same level before and after the third dose. Reciprocal 25% inhibition dilution titers in sVNT were approximately 1,000 two weeks after the second and third doses **(Figure 6i**), showing that vaccinated NHP plasma exhibited strong neutralization potential comparable with those of vaccinated mice (**Figure**

6d). Vaccinated NHPs showed a tendency of enhanced cellular immunity in IFN-γ ELISpot compared to the non-vaccinated control, although the difference lacks statistical significance because of high background values in the untreated control (**Supplementary Figure S3**). As is the case in mice, IL-4 spots were undetected. NHPs were also monitored for signs of reactogenicity and toxicity throughout the 8 weeks of the study. PYRO-injected NHPs with buffer or mRNA solution showed no change in body temperature 24 h after the prime and boost doses **(Figure 6j**) and undetectable systemic release of proinflammatory cytokines such as IL-6 and IFN-γ 24 h after the prime **(Figure 6k**). Throughout the observation period, body weight, hematology, and blood chemistry were comparable between mRNA-injected, buffer-injected, and untreated groups **(Figure 6l, supplementary table 2, 3**). These data demonstrate high safety and robust antibody response of naked mRNA PYRO injection in NHPs.

Discussion and conclusions

The skin contains a range of immune cells, making it a good target for vaccination. The repurposing of i.m. vaccines to the i.d. route in the recent Monkeypox virus outbreak in 2022 helped ameliorate supply shortages while ensuring similar levels of immunogenicity at lower doses (*45*). However, the successful introduction of naked antigen-encoding mRNA into the cutaneous tissue using hypodermic needles is usually hampered by the poor cellular uptake and stability of mRNA at the injection site (*27, 46*). The difficulty in inserting a hypodermic needle at the proper depth in small laboratory animals or humans and needles phobia are additional drawbacks (*47*). Notably, the fear of needle injection accounts for >10% of COVID-19 vaccine hesitancy cases (*48*). The physical introduction of naked nucleic acids aided by external force has long been investigated (*49*). Cutaneous electroporation is the most widely used to deliver pDNA or mRNA vaccines without an injection needle. However, electroporation requires bulky and complex instrumentation (*50, 51*), prompting the development of small-sized electroporators (*52*), or other portable i.d. injection technologies (*53*), for cheaper manufacturing and easier distribution of vaccines during pandemics.

Liquid jet injectors (LJIs) represent another important class for cutaneous immunization by delivering antigens across the stratum corneum driven by liquid jet pressure, overriding the cell toxicity associated with prolonged voltage pulses of electroporators (*54*). However, conventional LJI actuators, including those of the Lorentz force, are still bulky and incapable of precisely controlling the injection depth (*54, 55*). PYRO, a portable LJI operated by a miniaturized single actuator, controls the injection pressure using explosives with bi-phasic burning rates. The device is thereby useful in modulating the injection settings depending on the animal species, age, and dosage (*28*). Most importantly, the rapid pressure rise as a result of gas combustion expels the liquid in a high-speed stream, which aids not only in penetrating the skin but also delivering macromolecules intracellularly at the injection site. In this study, we utilized

PYRO as a delivery device to potentiate the efficacy of naked mRNA i.d. vaccines for the following reasons: (i) its capacity to deliver nucleic acids intracellularly (*29*), (ii) instantaneous delivery timeframe, which helps evade the rapid extracellular degradation of naked mRNA, (iii) portable size and easy operation for rapid deployment.

Using PYRO for efficient introduction of antigens only at the injection site in the skin, we, for the first time, separated the two action modes of mRNA vaccines; the local and systemic effects. Antigen expression from PYRO-injected naked mRNA was localized to the injection site without any systemic migration of mRNA on the one hand. LNP, on the other hand, provided strong antigen expression in the injection site and other organs, including dLN, spleen, and liver (**Figure 7**). Jet-injection of naked mRNA induced robust humoral and cellular immunity without any systemic vaccine spillage, highlighting that antigen expression in the injection site played a critical role in effective vaccination. As for the mechanisms in which naked mRNA induced a systemic adaptive immune response, we postulated that APCs that take up the antigen expressed in the skin migrate to the dLN, where they present the antigen to T and B cells (**Figure 7**). Indeed, microscopic imaging confirmed the accumulation of *GFP*-positive APCs in the inguinal dLN following the PYRO injection of naked *GFP* mRNA in the skin (**Figure 4f, g**). Importantly, naked mRNA circumvented the induction of proinflammatory cytokines in systemic organs even at higher doses, whereas the use of LNP may be hampered by excessive reactogenicity at high doses (**Figure 3**). Ultimately, the PYRO injection of naked mRNA outperformed the LNP in humoral immunity induction at the highest tolerable *OVA* mRNA doses of each formulation (9 μg for naked mRNA PYRO injection and 2 μg for LNP).

From a clinical point of view, enabling mRNA vaccines in the naked form can be promising due to its requirement for minimal formulation. Naked mRNA vaccines can be useful to avoid rare cases of hepatic autoimmunity (*14*) and allergic reactions (*56*) caused by mRNA-LNP vaccines and make repeated vaccine dosing possible to those at high risk. Normally, antibody levels correlate well with protection from COVID-19 infection (*57*), while cellular immunity is essential for preventing severe symptoms and deaths (*58*). PYRO-injected naked mRNA induced efficient humoral immunity against spike protein in mice and NHPs, holding promises for future COVID-19 vaccine development. Importantly, PYRO injection of naked mRNA showed no signs of reactogenicity or systemic toxicity in NHPs. The major limitation of naked mRNA jet injection is the weaker induction of cellular immunity relative to mRNA-LNP. This issue might be due to the lack of mRNA distribution to the dLN following jet injection. Further enhancement in the potency of PYRO injections will be addressed in the future, by tweaking other vaccine design parameters such as mRNA chemical modifications and using immunostimulatory adjuvants.

Materials and methods

1. Materials

CleanCap® *EGFP* mRNA, *firefly luciferase (fLuc)* mRNA, N1-Methylpseudouridine (m1Ψ)-modified *OVA* mRNA, and m1Ψ-modified spike mRNA with di-proline substitutions of K968 and V969 were obtained from Trilink biotechnologies (San Diego, CA, USA). The Actranza™ lab i.d. delivery device (PYRO) was purchased from Daicel Corporation (Tokyo, Japan). Ovalbumin (OVA) was purchased from Sigma Aldrich (St. Louis, MO, USA). A goat anti-mouse IgG HRP-conjugated antibody was bought from R&D systems (Minneapolis, MN) for OVA vaccination studies in C57BL/6 mice, and from Abcam (Cambridge, UK) for other mouse vaccination experiments. Goat anti-mouse IgG1, goat anti-mouse IgG2a, and Goat Anti-Monkey IgG conjugated with HRP were purchased from Abcam. Anti-IFNγ and anti-IL-4 ELISpot PLUS kits were purchased from Mabtech (Nacka Strand, Sweden). PepTivator Ovalbumin epitope mix was provided by Miltenyi Biotec (Nordrhein-Westfalen, Germany). PepMix™ SARS-CoV-2 (S) was obtained from JPT Peptide technologies (Berlin, Germany). Paraformaldehyde (PFA, 16%) was purchased from Alfa Aesar (Haverhill, MA, USA). SARS-CoV-2 Spike RBD-ACE2 Blocking Antibody Detection ELISA Kit was obtained from Cell Signaling Technologies.

2. LNP formulation

In a four-component ionizable lipid nanoparticle (LNP) preparation, an ethanolic solution of D-Lin-MC3-DMA, DSPC, cholesterol, and PEG2000-DMG (50:10:38.5:1.5 mol %) was rapidly mixed with 3 volumes of 50 mM sodium citrate buffer (pH=3) containing the mRNA at [amino groups in D-Lin-MC3-DMA (N)] / [phosphate groups in mRNA (P)] ratio of 5, using a microfluidic micromixer (NanoAssemblr, Precision NanoSystems Inc., Vancouver, BC, Canada) at a flow rate of 12 mL/min. The product was then diluted 40x in PBS and concentrated using 30kD centrifugal filters (Millipore, MA, USA) to remove the ethanol. Encapsulation efficiency was determined using Quant-it™ RiboGreen RNA Assay Kit (Thermo Fisher Scientific, Waltham, MA, USA). Particle size was measured using dynamic light scattering (DLS) using a diode laser (λ = 532 nm) with a scattering angle of 173◦ (Zetasizer Nano-ZS, Malvern Instruments, Worcestershire, UK).

3. IVIS imaging

Female C57BL/6J and Balb/C mice were obtained from Charles River Laboratories Inc., Yokohama, Japan, and used at 6-9 weeks of age. All mouse experiments are performed under the ethical guidelines of the Innovation Center of NanoMedicine (iCONM), Kawasaki Institute of Industrial Promotion (Kanagawa, Japan). A luciferase reporter assay was used to quantify protein expression following i.d. delivery of1 μg *fLuc* mRNA in C57BL/6J or Balb/C mice. For needle and syringe (N&S) injections, mouse fur was removed using Epilat cream at one flank, and 20 μL HEPES buffer (10 mM, pH 7.4) containing naked *fLuc* mRNA or mRNA LNP was injected using a 35-gauge needle (FastGene™ Nano Needle, Nippon Genetics, Tokyo, Japan). For PYRO injections, mouse fur was shaved, and 20 μL of the same buffer containing naked mRNA was injected following the manufacturer's protocol. Protein expression was then quantified at 4, 24, 48, and

72 h post-injection using in vivo imaging system (IVIS, PerkinElmer). At each time point, imaging was performed 10 min after intraperitoneal (i.p.) injection with 200 μL of 15 mg/mL luciferin substrate (Promega). The total flux of luminescence was calculated by gating a region of interest (ROI) at the injection site. For *ex vivo* organ imaging, after i.p. injection of luciferin substrate, lymph nodes, livers, or spleens were extracted and imaged using IVIS.

4. Histopathology and microscopy

For the quantification of protein expression in the skin following injection of 9 μg *EGFP* mRNA, around 1 cm^2 of the skin surrounding the injection site was excised and fixed in 4% PFA in PBS for 24 h. The skin was then cut into several strips each around 2 mm in width, immersed in paraffin, and cooled down to form blocks for sectioning. Draining lymph nodes proximal to the injection site were also collected 24 h post injection and treated same as described above. The samples were sliced at 4 μm thickness, stained with hematoxylin and eosin (H&E), and observed under the optical microscope. For immunofluorescent staining of the paraffin-embedded samples, EnVision system (DAKO) was used according to the protocols with 5 min autoclaving at 121 °C under pH 9.0. Overnight incubation was performed for labelling dendritic cells (DCs) by a rabbit anti-CD11c antibody (Cell Signaling, #97585, 500× dilution) and EGFP by goat anti-GFP antibody (Abcam, ab5450, 1000× dilution). On the next day, the sections were washed and a mixture of secondary antibodies composed of Alexa Fluor 568 rabbit anti–goat IgG and Alexa Fluor 488 goat anti–rabbit IgG (Invitrogen) were applied to labeled CD11c and EGFP, respectively. The sections were incubated for 1 h at room temperature, washed, and observed under the fluorescent microscope (Keyence, Osaka, Japan) after the addition of DAPI to stain the cell nuclei.

5. Quantitative PCR

For the quantification of *OVA* mRNA delivered to mouse organs following injection in the skin, lymph nodes, the liver, and spleen were extracted and homogenized by Multi-beads shocker at 2,000 rpm for 30 sec. Total RNA was extracted from the homogenates using an RNeasy mini kit (Qiagen, Hilden, Germany). After the removal of genomic DNA by enzymatic degradation, complementary DNA (cDNA) was obtained by reverse transcription using a ReverTraAce with gDNA remover kit (TOYOBO, Osaka, Japan). The products were run on a 7500 fast real-time PCR (Applied Biosystems) using FastStart Universal SYBR Green Master kit. For the quantification of *OVA* mRNA, a forward primer: GAACCAGATCACCAAGCCCA, and reverse primer: GTACAGCTCCTTCACGCACT were used. Proinflammatory cytokines in these organs were also measured by quantitative PCR (qPCR), as described above, using the following primers. IL-6 (Mm00446190_m1)：4331182, IFN (Mm00439552_s1)：4331182, and B-Actin：4352933E. Data were analyzed with a $2^{-\Delta Ct}$ method using β-actin gene as an

endogenous control housekeeping gene. Data of proinflammatory cytokines were presented after normalization to nontreated (NT) samples.

6. Mouse immunization studies

OVA mRNA or *spike* mRNA were dissolved in HEPES buffer (10 mM, pH=7.3) when injected in the naked form, while the mRNA-LNPs were dispersed in PBS. 20 μL of the solution containing a specific amount of mRNA was injected at both flanks, followed by a booster 3 weeks later. 2 weeks after the last injection, mice were euthanized, and blood was collected from the inferior vena cava in heparinized tubes. Blood plasma was obtained by centrifugation at 2,000 ×g for 10 min at 4 °C and stored at -80 °C until used. Spleens were also collected and processed for ELISpot assay as described in section 8.

7. Detection of mouse antibodies

Antibodies in the blood plasma were evaluated using enzyme-linked immunosorbent (ELISA). For the detection of antigen-specific antibodies, OVA or recombinant spike protein were dissolved at 2 μg/mL in carbonate buffer (50 mM, pH=9.6). 50 μL/well of protein solution was added into Clear Flat-Bottom Immuno Nonsterile 96-Well Plates (Thermo). After overnight incubation at 4 °C, the plates were washed 3 times with 0.5% v/v Tween 20 in PBS (PBS-T). A 100 μL diluent of 1% BSA and 2.5 mM EDTA in PBS-T was added to each well and further incubated for 1 h at 23 °C. After removing the diluent, 50 μL blood plasma that was serially diluted in the same diluent was added to each well. The plates were incubated overnight at 4 °C, before washing 3 times with PBS-T. A 50μL of goat anti-mouse IgG (1:8000), IgG1 (1:10000), or IgG2a (1:10000) HRP-conjugated antibodies were added to each well and incubated for an additional 2 h at 23 °C. Finally, 100 μL/well of the HRP substrate was added and incubated for 30 min at 23 °C away from light. The reaction was stopped by adding 2M sulfuric acid, followed by measuring absorbance of 492 nm using a plate reader (Tecan, Switzerland). The detection of antibodies that block the interaction between the receptor-binding domain (RBD) of the SARS-CoV-2 spike protein and angiotensin converting enzyme 2 (ACE2) was measured by sVNT using a SARS-CoV-2 Spike RBD-ACE2 Blocking Antibody Detection ELISA Kit following the manufacturer's protocol.

8. ELISpot assay

Spleens from immunized mice were collected and disintegrated separately using a steel grid mesh with 5 mL of RPMI-1640 medium containing 10% FBS, 1 mM sodium pyruvate, 10 mM HEPES, 50 μM mercaptoethanol, and 1% penicillin/streptomycin. The suspension was then passed through a 40 μm nylon mesh (Cell strainer, Falcon) to form a single-cell suspension. Splenocytes were seeded at a density of 2.5×10^5 cell/well in anti-IFNγ or anti-IL-4-ELISpot 96 well plates and stimulated by the addition of 10 μL epitope mixture dissolved in PBS (0.025 μg/well OVA epitope mix and 0.2 μg/well spike epitope mix). The plates were incubated at 37 °C and 5% CO_2 overnight. The next day, the plates were washed and treated

according to the manufacturer's protocol. Spots were counted on an ELISpot plate reader (AID GmBH, Germany).

9. NHP immunization studies

NHP experiments were performed by Ina Resaerch Inc. (Nagano, Japan) under Act on Welfare and Management of Animals and animal experimental guidelines (Nagano, Japan) after being approved by Institutional Animal Care and Use Committee in Ina Research Inc. Cynomolgus monkeys (female, 3 – 4 years old) received 50 μL of lactated Ringer's buffer or mRNA solution (100 μg/mouse) at a single position at their back in each prime and boost dosing. ELISA assay was performed as described in section 7 except for using Goat Anti-Monkey IgG H&L (HRP) for detecting monkey IgG. Titers were determined as the highest dilution that showed absorbance optical density > 0.15. sVNT was performed as described in section 7. Titers were determined as the highest dilution that showed binding inhibition >25%. Peripheral blood mononuclear cells (PBMCs) were collected for ELISpot assays using ELISpot Plus: Monkey IFN-γ (HRP) and ELISpot Plus: Human IL-4 (HRP) kits (Mabtech). 2×10^5 PBMCsseeded onto 96 well plates in the kits were incubated with 1 μg of PepMix™ SARS-CoV-2 (Spike Glycoprotein) for 20 h followed by counting spot numbers using IMMUNOSPOT S6 Versa (Cellular Technology Ltd., Cleveland, OH). Safety analyses were performed using XN-2000 (Sysmex, Kobe, Japan), CA-510 (Sysmex) and flow cytometer (FACS Canto II, Becton, Dickinson and Company, Franklin Lakes, NJ) for measuring blood cell counts and coagulation functions, type 7180 auto analyzing machine (Hitachi, Tokyo, Japan) for blood chemistry analyses, and BD™ Cytometric Beads Array (CBA) Non-Human Primate Th1/Th2 Cytokine Kit (Becton, Dickinson and Company) for blood cytokine measurement.

10. Data representation

The statistical significance between the two groups was analyzed using an unpaired, two-tailed Student's *t*-test. Multiple comparisons between three or more groups were performed using non-repeated ANOVA followed by SNK post hoc test. Comparison against NT samples was performed using Dunette's test. A statistically significant difference was set at $p < 0.05$.

Acknowledgement

This work was supported by the Center of Innovation Program (COI) and COI accelerating support from Japan Science and Technology Agency (JST), Grants-in-Aid for Challenging Research (Pioneering) [18H05378 to K.K.], and for Scientific Research (A) [21H04962 to S.U., 21H04967 to K.K.] from the Ministry of Education, Culture, Sports, Science and Technology, Japan (MEXT), Leading Advanced Projects for Medical Innovation [21gm0010008s0101 to S.U.], and Research Program on Emerging and Re-emerging Infectious Diseases [21fk0108620h0001 to S.U.] from Japan Agency for Medical Research and Development (AMED). We would like to thank Yuki Sato, Keisuke Nagao, Yuki Tada (iCONM),

Satomi Nakagahara (NanoCarrier Ltd.), Ayumi Sumiishi, Namiko Kondo and Kaoruko Kojima (Kyorin University School of Medicine) for their technical assistance, Dr. Hiroaki Shimoyamada (Kyorin University School of Medicine) for his consultation about histological evaluation, Dr. Katsumi Takaba (Skypatho) for his consultation about NHP experiments, Daicel Corporation for the assistance in jet injection and Ina Research Inc. for performing NHP experiments.

Competing Interest Statement: Sa.A., M.M., H.A., K.K., and S.U. have filed a patent application related to this study, and NanoCarrier Ltd. (M.M., Sh.A.) holds a right to the patent. K.K. is a founder and a member of the Board of NanoCarrier Ltd. M.M. is an employee of NanoCarrier Ltd. Sh.A. is a CEO and CSO of NanoCarrier Ltd.

References

1. N. Pardi, M. J. Hogan, F. W. Porter, D. Weissman, mRNA vaccines - a new era in vaccinology. *Nat. Rev. Drug Discov.* **17**, 261-279 (2018).
2. N. Chaudhary, D. Weissman, K. A. Whitehead, Author Correction: mRNA vaccines for infectious diseases: principles, delivery and clinical translation. *Nat Rev Drug Discov* **20**, 880 (2021).
3. L. R. Baden *et al.*, Efficacy and Safety of the mRNA-1273 SARS-CoV-2 Vaccine. *N Engl J Med* **384**, 403-416 (2021).
4. K. S. Corbett *et al.*, SARS-CoV-2 mRNA vaccine design enabled by prototype pathogen preparedness. *Nature* **586**, 567-571 (2020).
5. F. P. Polack *et al.*, Safety and Efficacy of the BNT162b2 mRNA Covid-19 Vaccine. *N Engl J Med* **383**, 2603-2615 (2020).
6. E. E. Walsh *et al.*, Safety and Immunogenicity of Two RNA-Based Covid-19 Vaccine Candidates. *N Engl J Med* **383**, 2439-2450 (2020).
7. N. Pardi *et al.*, Expression kinetics of nucleoside-modified mRNA delivered in lipid nanoparticles to mice by various routes. *J. Control. Release* **217**, 345-351 (2015).
8. K. J. Hassett *et al.*, Optimization of Lipid Nanoparticles for Intramuscular Administration of mRNA Vaccines. *Mol Ther Nucleic Acids* **15**, 1-11 (2019).
9. J. Di *et al.*, Biodistribution and Non-linear Gene Expression of mRNA LNPs Affected by Delivery Route and Particle Size. *Pharm Res* **39**, 105-114 (2022).
10. R. Verbeke, M. J. Hogan, K. Lore, N. Pardi, Innate immune mechanisms of mRNA vaccines. *Immunity* **55**, 1993-2005 (2022).
11. W. Kim *et al.*, Germinal centre-driven maturation of B cell response to mRNA vaccination. *Nature* **604**, 141-145 (2022).
12. K. Roltgen *et al.*, Immune imprinting, breadth of variant recognition, and germinal center response in human SARS-CoV-2 infection and vaccination. *Cell* **185**, 1025-1040 e1014 (2022).

13. I. P. Trougakos *et al.*, Adverse effects of COVID-19 mRNA vaccines: the spike hypothesis. *Trends Mol. Med.* **28**, 542-554 (2022).
14. T. Boettler *et al.*, SARS-CoV-2 vaccination can elicit a CD8 T-cell dominant hepatitis. *J. Hepatol.* **77**, 653-659 (2022).
15. S. Uchida, F. Perche, C. Pichon, H. Cabral, Nanomedicine-Based Approaches for mRNA Delivery. *Mol. Pharm.* **17**, 3654-3684 (2020).
16. S. G. Reed, M. T. Orr, C. B. Fox, Key roles of adjuvants in modern vaccines. *Nat. Med.* **19**, 1597-1608 (2013).
17. C. Caudill *et al.*, Transdermal vaccination via 3D-printed microneedles induces potent humoral and cellular immunity. *Proc. Natl. Acad. Sci. U. S. A.* **118**, (2021).
18. B. Petsch *et al.*, Protective efficacy of in vitro synthesized, specific mRNA vaccines against influenza A virus infection. *Nature Biotechnol.* **30**, 1210-1216 (2012).
19. M. Alberer *et al.*, Safety and immunogenicity of a mRNA rabies vaccine in healthy adults: an open-label, non-randomised, prospective, first-in-human phase 1 clinical trial. *The Lancet* **390**, 1511-1520 (2017).
20. N. Pardi *et al.*, Zika virus protection by a single low-dose nucleoside-modified mRNA vaccination. *Nature* **543**, 248-251 (2017).
21. G. V. T. Roozen *et al.*, Tolerability, safety and immunogenicity of intradermal delivery of a fractional dose mRNA-1273 SARS-CoV-2 vaccine in healthy adults as a dose sparing strategy. *medRxiv*, 2021.2007.2027.21261116 (2021).
22. P. Intapiboon *et al.*, Immunogenicity and Safety of an Intradermal BNT162b2 mRNA Vaccine Booster after Two Doses of Inactivated SARS-CoV-2 Vaccine in Healthy Population. *Vaccines (Basel)* **9**, (2021).
23. R. Sophonmanee *et al.*, T-Cell Responses Induced by an Intradermal BNT162b2 mRNA Vaccine Booster Following Primary Vaccination with Inactivated SARS-CoV-2 Vaccine. *Vaccines (Basel)* **10**, (2022).
24. J. P. Carralot *et al.*, Polarization of immunity induced by direct injection of naked sequence-stabilized mRNA vaccines. *Cell. Mol. Life Sci.* **61**, 2418-2424 (2004).
25. A. Selmi *et al.*, Uptake of synthetic naked RNA by skin-resident dendritic cells via macropinocytosis allows antigen expression and induction of T-cell responses in mice. *Cancer Immunol Immunother* **65**, 1075-1083 (2016).
26. S. Kreiter *et al.*, Intranodal vaccination with naked antigen-encoding RNA elicits potent prophylactic and therapeutic antitumoral immunity. *Cancer Res.* **70**, 9031-9040 (2010).
27. J. Probst *et al.*, Characterization of the ribonuclease activity on the skin surface. *Genet. Vaccines Ther.* **4**, 4 (2006).
28. H. Miyazaki, S. Atobe, T. Suzuki, H. Iga, K. Terai, Development of Pyro-Drive Jet Injector With Controllable Jet Pressure. *J. Pharm. Sci.* **108**, 2415-2420 (2019).
29. C. Chang *et al.*, Stable Immune Response Induced by Intradermal DNA Vaccination by a Novel Needleless Pyro-Drive Jet Injector. *AAPS PharmSciTech* **21**, 19 (2019).
30. T. Nishikawa *et al.*, Anti-CoVid19 plasmid DNA vaccine induces a potent immune response in rodents by Pyro-drive Jet Injector intradermal inoculation. *bioRxiv*, 2021.2001.2013.426436 (2021).
31. S. Inoue *et al.*, Induction of potent antitumor immunity by intradermal DNA injection using a novel needle-free pyro-drive jet injector. *Cancer Sci.* **114**, 34-47 (2023).

32. H. Zhang *et al.*, Fluorescence-Based Quantification of Messenger RNA and Plasmid DNA Decay Kinetics in Extracellular Biological Fluids and Cell Extracts. *Adv Biosyst* **4**, e2000057 (2020).
33. D. An *et al.*, Systemic Messenger RNA Therapy as a Treatment for Methylmalonic Acidemia. *Cell Rep.* **21**, 3548-3558 (2017).
34. R. Verbeke, I. Lentacker, S. C. De Smedt, H. Dewitte, The dawn of mRNA vaccines: The COVID-19 case. *J. Control. Release* **333**, 511-520 (2021).
35. T. Nakamura, H. Harashima, Dawn of lipid nanoparticles in lymph node targeting: Potential in cancer immunotherapy. *Adv. Drug. Deliv. Rev.* **167**, 78-88 (2020).
36. S. Abbasi, S. Uchida, Multifunctional Immunoadjuvants for Use in Minimalist Nucleic Acid Vaccines. *Pharmaceutics* **13**, (2021).
37. L. M. Hook *et al.*, Antibodies to Crucial Epitopes on HSV-2 Glycoprotein D as a Guide to Dosing an mRNA Genital Herpes Vaccine. *Viruses* **14**, (2022).
38. U. Sahin *et al.*, COVID-19 vaccine BNT162b1 elicits human antibody and TH1 T cell responses. *Nature* **586**, 594-599 (2020).
39. C. Li *et al.*, Mechanisms of innate and adaptive immunity to the Pfizer-BioNTech BNT162b2 vaccine. *Nat. Immunol.* **23**, 543-555 (2022).
40. M. S. Gebre *et al.*, Optimization of non-coding regions for a non-modified mRNA COVID-19 vaccine. *Nature* **601**, 410-414 (2022).
41. J. F. Nicolas, B. Guy, Intradermal, epidermal and transcutaneous vaccination: from immunology to clinical practice. *Expert Rev Vaccines* **7**, 1201-1214 (2008).
42. H. W. Lee *et al.*, Tracking of dendritic cell migration into lymph nodes using molecular imaging with sodium iodide symporter and enhanced firefly luciferase genes. *Sci Rep* **5**, 9865 (2015).
43. B. F. Haynes *et al.*, Prospects for a safe COVID-19 vaccine. *Sci. Transl. Med.* **12**, eabe0948 (2020).
44. C. W. Tan *et al.*, A SARS-CoV-2 surrogate virus neutralization test based on antibody-mediated blockage of ACE2-spike protein-protein interaction. *Nature Biotechnol.* **38**, 1073-1078 (2020).
45. J. T. Brooks, P. Marks, R. H. Goldstein, R. P. Walensky, Intradermal Vaccination for Monkeypox - Benefits for Individual and Public Health. *N Engl J Med* **387**, 1151-1153 (2022).
46. H. Huysmans *et al.*, Expression Kinetics and Innate Immune Response after Electroporation and LNP-Mediated Delivery of a Self-Amplifying mRNA in the Skin. *Mol Ther Nucleic Acids* **17**, 867-878 (2019).
47. A. Wilder-Smith, S. Desai, A. Cravioto, H. Nohynek, J. Hombach, Caution before fractionating COVID-19 vaccines. *Nat Med* **27**, 1856-1857 (2021).
48. D. Freeman *et al.*, Injection fears and COVID-19 vaccine hesitancy. *Psychol Med*, 1-11 (2021).
49. T. K. Kim, J. H. Eberwine, Mammalian cell transfection: the present and the future. *Anal Bioanal Chem* **397**, 3173-3178 (2010).
50. A. R. Denet, R. Vanbever, V. Preat, Skin electroporation for transdermal and topical delivery. *Adv Drug Deliv Rev* **56**, 659-674 (2004).

51. D. X. Johansson, K. Ljungberg, M. Kakoulidou, P. Liljestrom, Intradermal electroporation of naked replicon RNA elicits strong immune responses. *PLoS One* **7**, e29732 (2012).
52. D. Xia *et al.*, An ultra-low-cost electroporator with microneedle electrodes (ePatch) for SARS-CoV-2 vaccination. *Proc. Natl. Acad. Sci. U. S. A.* **118**, (2021).
53. A. Khobragade *et al.*, Efficacy, safety, and immunogenicity of the DNA SARS-CoV-2 vaccine (ZyCoV-D): the interim efficacy results of a phase 3, randomised, double-blind, placebo-controlled study in India. *Lancet* **399**, 1313-1321 (2022).
54. S. Mitragotri, Current status and future prospects of needle-free liquid jet injectors. *Nat Rev Drug Discov* **5**, 543-548 (2006).
55. A. Taberner, N. C. Hogan, I. W. Hunter, Needle-free jet injection using real-time controlled linear Lorentz-force actuators. *Med Eng Phys* **34**, 1228-1235 (2012).
56. R. Shavit *et al.*, Prevalence of Allergic Reactions After Pfizer-BioNTech COVID-19 Vaccination Among Adults With High Allergy Risk. *JAMA Netw Open* **4**, e2122255 (2021).
57. D. S. Khoury *et al.*, Neutralizing antibody levels are highly predictive of immune protection from symptomatic SARS-CoV-2 infection. *Nat. Med.* **27**, 1205-1211 (2021).
58. A. T. Tan *et al.*, Early induction of functional SARS-CoV-2-specific T cells associates with rapid viral clearance and mild disease in COVID-19 patients. *Cell Rep.* **34**, 108728 (2021).

Figures

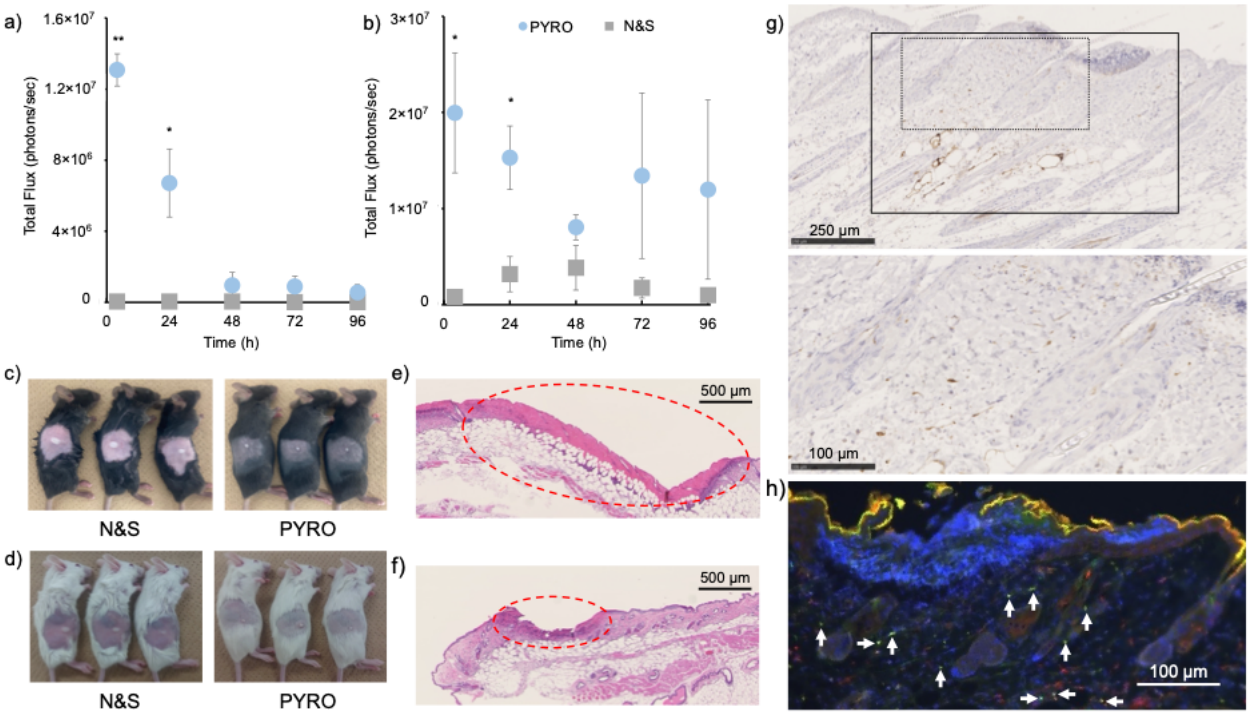

Figure 1. PYRO injection of naked mRNA in mouse skin. (a, b) Luciferase expression quantified by IVIS imaging following i.d. injection of naked mRNA in the right flank of C57BL/6J **(a)** and Balb/C mice **(b)**. Data represent the mean ± SEM (n=3). $^{**}p<0.01$, $^{*}p<0.05$, unpaired Student's *t*-test. **(c, d)** The appearance of injection site after i.d. injection of naked mRNA using N&S and PYRO in C57BL/6J **(c)** and Balb/C mice **(d)**. **(e, f)** Tissue sections stained using H&E collected 24 h after i.d. injection of naked mRNA using N&S **(e)** and PYRO **(f)** in Balb/C mice. **(g, h)** Tissue distribution of GFP expression 24 h after PYRO injection of naked mRNA. **(g)** GFP was stained in brown by immunohistology. A solid rectangle shows the area containing GFP-positive cells. The bottom figure shows the magnification of the dotted rectangle in the upper figure. **(h)** GFP expression in dendritic cells was confirmed by staining GFP in green and CD11c in red. White arrows indicate the colocalization of GFP and CD11c.

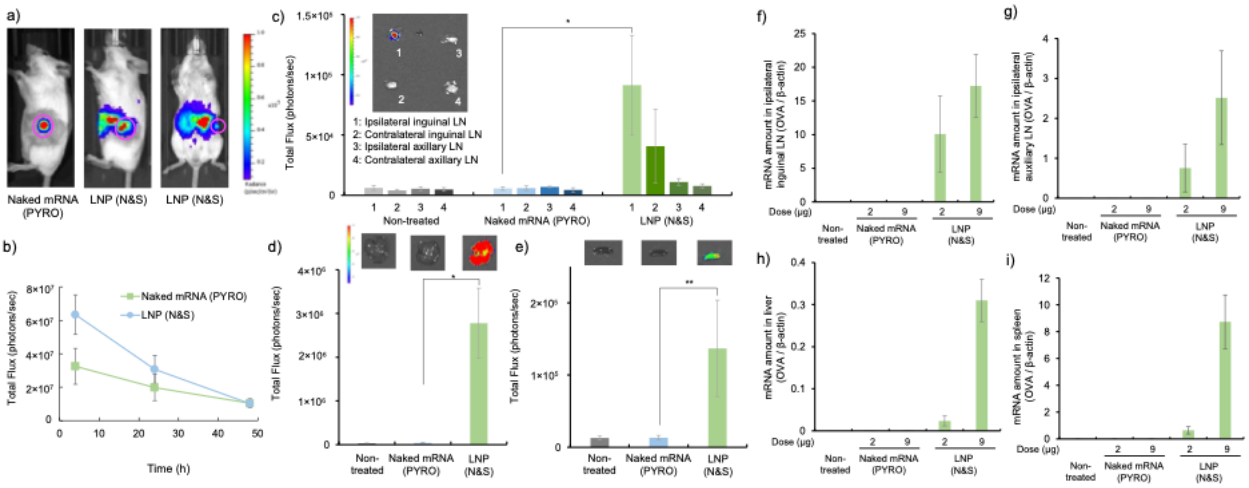

Figure 2. Distribution of protein expression and mRNA after PYRO injection and LNP delivery. (a-b) Whole body IVIS imaging of Balb/C mice. **(a)** Representative images obtained 4 h after the injection. Expression at the injection site is encircled in pink. **(b)** Quantification of luciferase expression levels at the injection site. **(c-e)** Luciferase levels in extracted tissues quantified by IVIS imaging 24 h post-injection. **(c)** Inguinal and axillary LNs on the same side (ipsilateral side) and the opposite side (contralateral side) of the injection site. **(d)** The liver. **(e)** The spleen. Data represent the mean ± SEM (n=3-4). $^{**}p<0.01$, $^{*}p<0.05$, unpaired Student's *t*-test. **(f-i)** Tissue distribution of *OVA* mRNA 4 h after its PYRO injection in the naked form or N&S injection in the LNP form. *OVA* mRNA amounts in the tissues were normalized to *β-actin* mRNA amounts by qPCR. **(f)** The ipsilateral inguinal LN. **(g)** The ipsilateral auxiliary dLN. **(h)** The liver. **(i)** The spleen. Data represent the mean ± SEM (n=5-6).

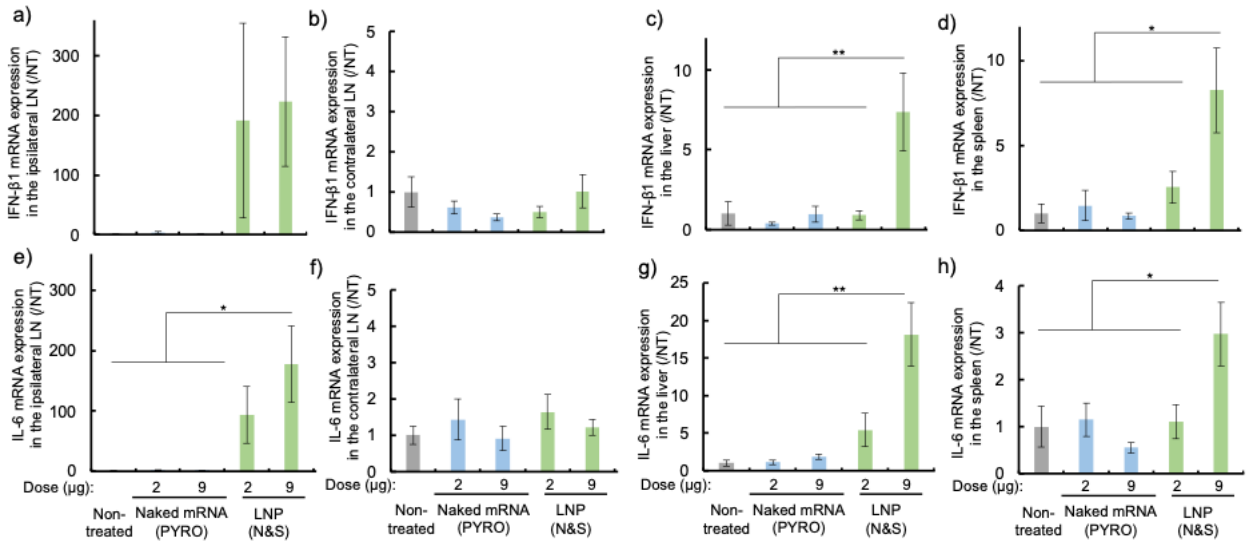

Figure 3. Proinflammatory response after PYRO injection and LNP delivery. Proinflammatory transcript levels in each tissue were measured with qPCR 4 h after PYRO injection of naked mRNA or N&S injection of LNPs. The levels are normalized to non-treated samples (NT). **(a-d)** INF-β1. **(e-h)** IL-6. **(a, e)** The inguinal LN ipsilateral to the injection site. **(b, f)** The inguinal LN contralateral to the injection site. **(c, g)** The liver. **(d, h)** The spleen. Data represent the mean ± SEM (n=5-6). $^{**}p<0.01$, $^{*}p<0.05$, non-repeated ANOVA followed by SNK test.

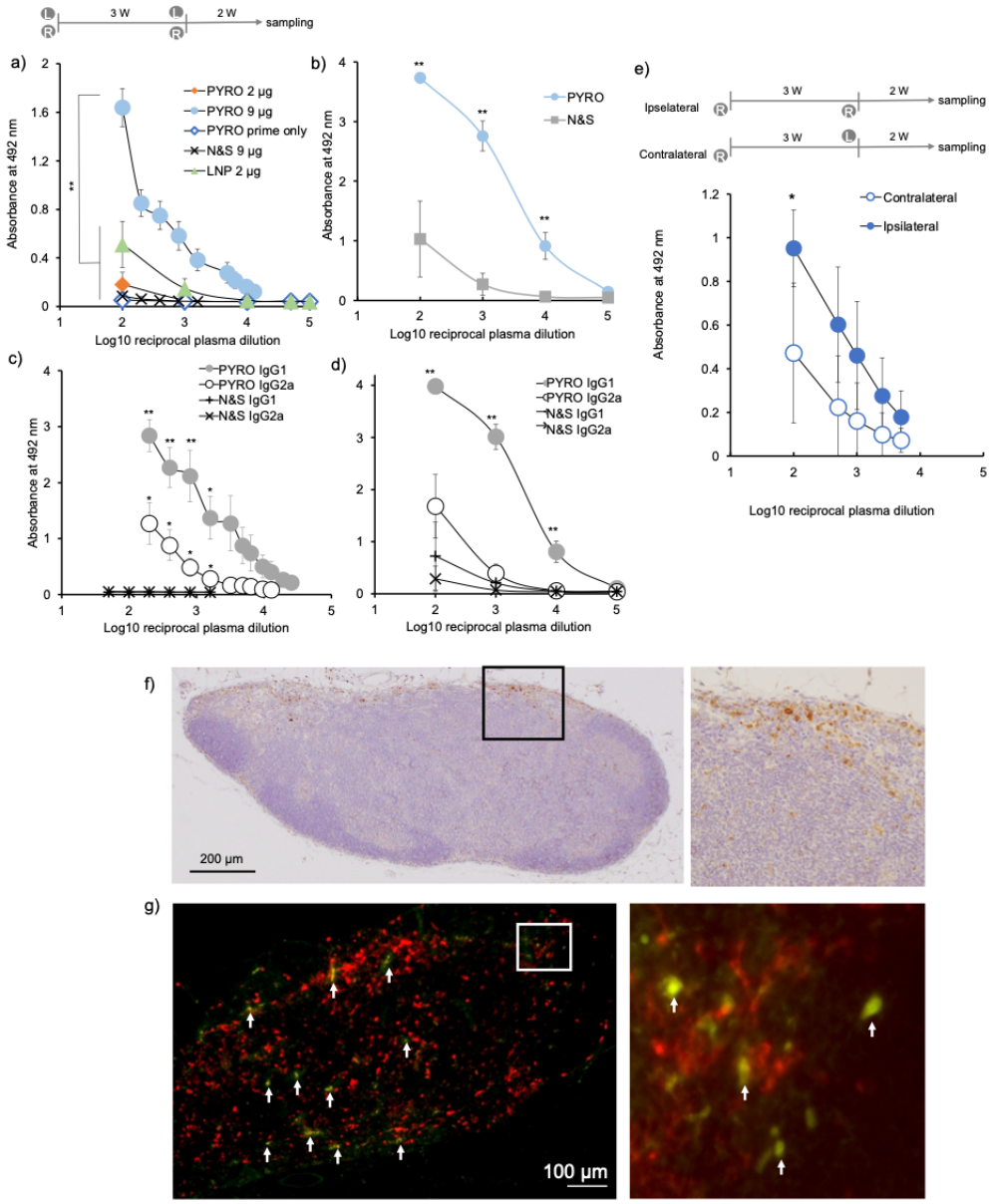

Figure 4. Humoral immunity against OVA. (a-e) Absorbance vs. plasma dilution curves in anti-OVA IgG ELISA in **(a,c,e)** C57BL/6J and **(b,d)** Balb/C mice. Mice were immunized twice at a 3-week interval, except for the prime-only group in **(a)**. Blood plasma is collected 5 weeks after the prime. Naked mRNA injected by PYRO or N&S, or LNP injected by N&S, were administered into both flanks each time in **(a-d)**. The prime and boost doses were administered to only one flank each time to see the effect of the injection side on antibody production in **(e)**. Data represent the mean ± SEM. n = 4 in **(a-d)**. n = 5 – 6 in **(e)**. Statistical analyses were performed by non-repeated ANOVA followed by SNK test in **(a)** and unpaired Student's *t*-test in **(b-e)**. $^{**}p<0.01$, $^{*}p<0.05$. PYRO IgG1 vs. N&S IgG1 and PYRO IgG2a vs. N&S IgG2a in **(c, d)**. **(f, g)** Inguinal dLN imaging 24 h after PYRO-injection of naked GFP mRNA in the skin of Balb/C mice. **(f)** GFP was stained brown. **(g)** GFP expression in dendritic cells was observed by staining GFP in green and CD11c in red. White arrows indicate the colocalization of the GFP and CD11c.

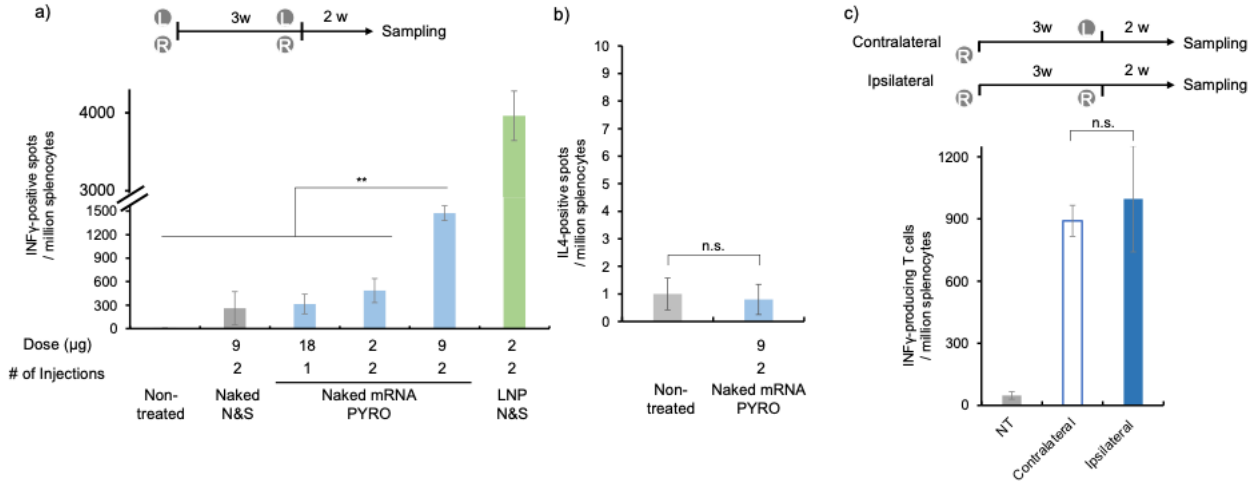

Figure 5. Cellular immunity against OVA. C57BL/6J mice were immunized twice at a 3-week interval on both sides for each prime and boost in **(a,b)** and on one side in **(c)**. Splenocytes were collected 5 weeks after the prime for ELISpot assay, using total splenocytes. Data represent the mean ± SEM. n = 4 in **(a,b)**. n = 5 – 6 in **(c)**. Statistical analyses were performed by non-repeated ANOVA followed by SNK test in **(a)** and unpaired Student's *t*-test in **(b,c)**. $^{**}p<0.01$, $^{*}p<0.05$. n.s.: non-significant.

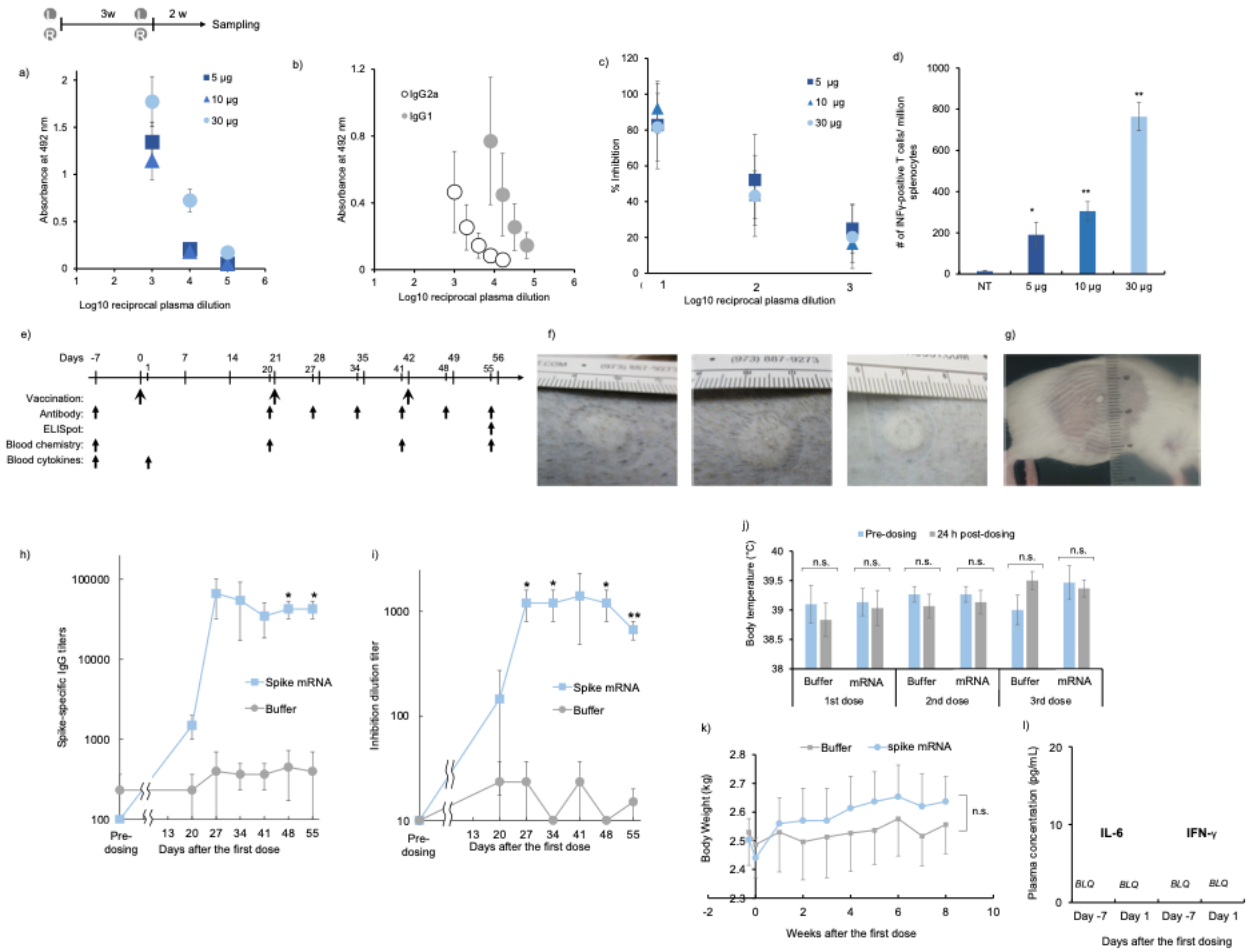

Figure 6. Immunity and safety evaluation of naked *spike* mRNA injected using PYRO. (a-d) Balb/C mice were PYRO-injected with naked *spike* mRNA at both flanks in a prime-boost setting separated by a 3-week interval. 5 weeks after the prime, blood plasma and splenocytes were collected for evaluating humoral and cellular immunity. **(a,b)** Anti-spike IgG ELISA absorbance vs. plasma dilution curves**. (c)** The ability of plasma in blocking the binding between spike-RBD and ACE2 proteins. **(d)** Quantification of spike-specific INFγ-positive splenocytes. Data represent the mean ± SEM (n=4). $^{**}p<0.01$, $^{*}p<0.05$ vs. NT, non-repeated ANOVA followed by Dunnett's test in **(d)**. **(e-l)** Vaccination in NHPs. **(e)** Injections and sampling schedule. **(f,g)** Appearance of PYRO injection site on the back of Cynomolgus monkeys **(f)** compared to Balb/C mice **(g)**. **(h)** Anti-spike IgG titers in NHPs PYRO-injected with buffer or mRNA solution. **(i)** Binding inhibition of ACE2 and SARS-CoV-2 RBD by plasma of immunized monkeys. **(j-l)** Toxicity evaluation in PYRO-injecting monkeys receiving either buffer or spike mRNA. **(j)** Body temperature measured immediately before and 24 h post dosing, after each of the 3 doses. **(k)** Change in body weight. **(l)** Plasma levels of proinflammatory cytokines before and 24 h after the first dose. n.s.: non-significant, $^{**}p<0.01$, $^{*}p<0.05$ vs. buffer treatment in unpaired Student's *t*-test. BLQ: below limit of quantification.

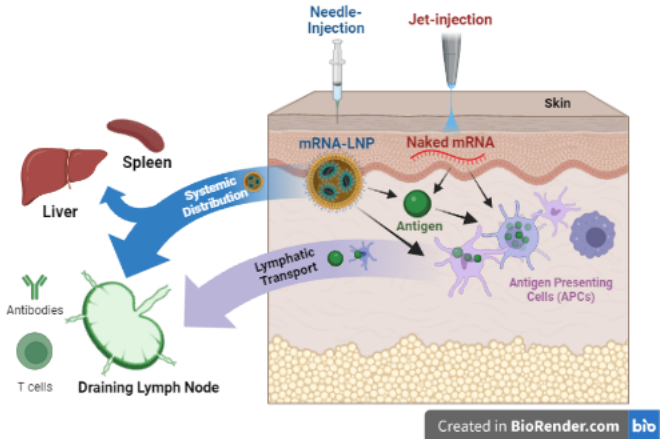

Figure 7. Illustration showing the difference in the mechanisms of intradermal naked mRNA vaccines delivered using PYRO compared to LNP-mediated delivery.